forum acusticum 2026
8-12 September · Graz, Austria

EXPERIMENTAL INVESTIGATION OF THE NOISE RADIATION OF AN ELECTRIC MOTOR FOR URBAN AIR MOBILITY VEHICLES

Philipp Schulze, Erik W. Schneehagen and Thomas F. Geyer

German Aerospace Center (DLR), Institute of Electrified Aero Engines

Abstract

The electrification of the aviation sector requires new propulsion technologies for future aircraft concepts. A key component of these systems is the electric motor, which converts electrical energy into mechanical power for the propulsor (e.g., open rotors or ducted fans). Within the DLR project VIRLWINT, the psychoacoustic effects of two urban air mobility (UAM)vehicles equipped with electric propulsion systems are investigated. To improve understanding of the electric propulsion system's contribution to overall aircraft noise, acoustic measurements were conducted on a representative electric motor. These measurements were performed under poor acoustic conditions, with significant background noise and sound-reflecting boundaries. The analysis focuses on the noise characteristics of the electric machine under varying operating conditions, such as rotational speed and load. A local regression algorithm was used to obtain the broadband noise from the dominant tonal features of the spectra. The results indicate that rotational speed influences the amplitude of both tonal and broadband noise components, whereas changes in torque affect only the tonal components, leaving the broadband noise largely unchanged.

Keywords: *electric motor noise, urban air mobility, measurement*

1. Introduction

The electrification of the aviation sector may be a key technology for reducing emitted pollutants. However, this new technology involves potential new sources of noise, which can affect its social acceptance. To facilitate understanding of noise generation in electric aircraft propulsion systems during the early design phase, studies are necessary to investigate the mechanisms that produce noise. In the DLR project VIRLWINT ("Virtueller akustischer Zwilling verteilter Antriebe"), the psychoacoustic effects of two UAM vehicles driven by electric distributed propulsion systems are being investigated [1]. The power requirements for the electric motor examined in the current study were determined based on the two UAM concepts. While numerous numerical and analytical methods exist to estimate the sound radiation of electric motors [2], acoustic measurements under varying load conditions are less often performed in research. In this study, a representative drive train was used to measure an electric motor under different load conditions in relation to noise radiation. In the final phase of the project, the resulting digital auralizations will be evaluated through laboratory listening tests with human subjects.

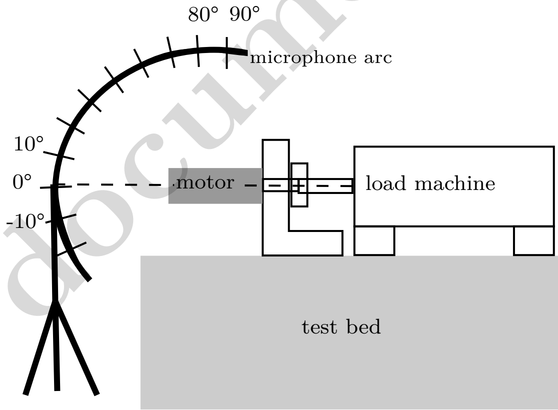

Figure 1: Scematic presentation of the test setup, side view.

Based on the power requirements for the electric drive train and the operating points for the flyover scenarios of both vehicle concepts, the specifications of the electric motor needed to best cover both variants was analyzed. For the procured motor, it was additionally

Corresponding author: *philipp.schulze@dlr.de.*

Table 1: Specifications of the investigated motor. [3]

cont. power	93 kW
nom. speed	20000 min^{-1}
cont. torque	60 Nm
max. power	200 kW
max. torque	120 Nm
number of pole pairs	4
number of slots	48

considered that the efficiency and power-to-weight ratio should correspond to forecasts for future motors needed in aviation. The motor under investigation is a permanent magnet synchronous motor with radially oriented magnetic flux. The specifications of the motor are listed in Table 1. The results presented in this work only refer to the electric motor and are representative of the drive train, as it is assumed that the motor is the dominant source of noise. A psychoacoustic analysis of the results is not part of this work.

2. Experimental setup

The measurements were carried out in an electric motor test bench intended for power testing. In this acoustically poor measurement environment it was not possible to separate the motor from other sound-radiating components and installations, such as the load machine or the cooling-water pump. Moreover, the test bench contains many reflective surfaces. These two factors create challenging conditions for the acoustic measurements. The used measurement setup is illustrated in a schematic presentation in Figure 1. The motor was fixed on the same test bed as the load machine and connected to it with a shaft clutch combination. For the microphone positioning during the measurements, an arc with radius $r = 1.2$ m was chosen. The microphones had a distance of 10° in peripheral distance. Figure 2 show a photograph of the measurement setup. It can be seen that additional sound absorbing foam was placed around the motor to reduce direct reflections. The far field condition is $f_{\text{far}} > 297$ Hz.
The microphone signals were recorded with a 24-channel data acquisition system with a sampling frequency of 100 kHz. In addition to the microphone signals, the signals of three triaxial accelerometers placed on the surface of the motor were collected synchronously with the same system. One of these accelerometers is vertically aligned with the microphone located at 90° along its z-direction. The measurement duration was 60 s.

3. Methods

3.1. Measurements

To investigate the acoustic behaviour of the motor under different load conditions, the motor was tested using the operating parameters listed in Tables 2 and 3. All measurements can be categorized into two groups,

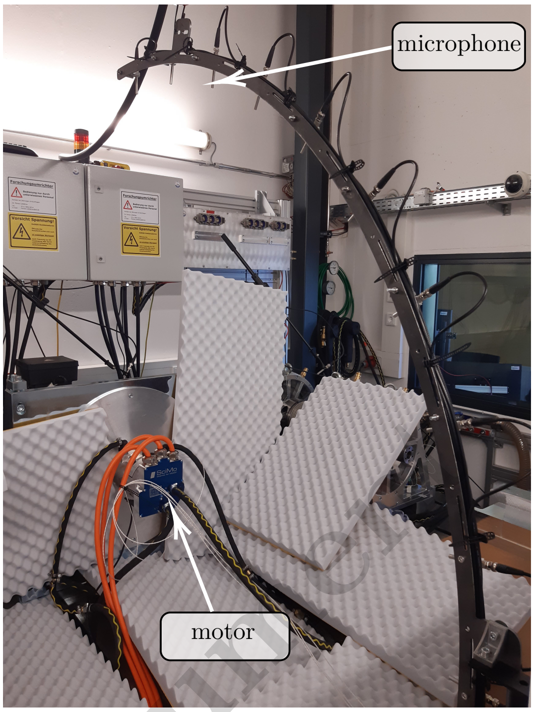

Figure 2: Photograph of the measurement setup in the electric motor teststand.

Table 2: Operating points with constant torque at different rotational speeds.

Torque	0 Nm	60 Nm	90 Nm
speed	840 min^{-1}	840 min^{-1}	840 min^{-1}
	3000 min^{-1}	3000 min^{-1}	3000 min^{-1}
	6000 min^{-1}	6000 min^{-1}	6000 min^{-1}
	7800 min^{-1}	7800 min^{-1}	7800 min^{-1}

(1) constant torque with varying speeds and (2) constant speed with varying torques.

3.2. Data processing

For the analysis the fast Fourier transformation (FFT) was carried out using Welch´s method [4]. A frequency spacing of 3.05 Hz was achieved using a Hanning window and 32,768 samples per block. The overlap was set to 50 % and leads to 365 blocks. This leads to relative errors of the amplitude of 0.05 [5].
To improve the separation of motor-radiated noise from background noise, several methods were tested. The first approach involved background-noise subtraction. Therefore the auto spectral density G_{xx} measured on the load machine alone (at the same rotational speed) was subtracted from the auto spectral density obtained from the far-field noise measurement at the operating points.
The second approach that was tested employed the Coherent Output Power (COP) method [5], which assumes that surface vibration and radiated noise of the motor under test are coherent when the noise is caused by the vibrations. Assuming that the accelerometer

Table 3: Operating points for constant rotational speed at 3000 min-1 and 6000 min-1 and different load conditions.

speed	3000 min-1	6000 min-1
torque	0 Nm	0 Nm
	15 Nm	15 Nm
	30 Nm	30 Nm
	45 Nm	45 Nm
	60 Nm	60 Nm
	75 Nm	75 Nm
	90 Nm	90 Nm

Table 4: Order of the fundamental harmonics for an electric motor [7], [8].

mechanism	order
space harmonics of the stator	40; 56
space harmonics of the rotor	8; 24
winding of the stator and space harmonics of the rotor	32; 64
interaction of rotor magnetic field and the stator slots	0; 192
cogging torque	12

is unaffected by external noise sources, only motor-generated tonal noise remains coherent, while noise at other frequencies, originating from interfering sources and captured by the microphone, exhibits reduced coherence.

A third method used in this work is a locally weighted regression using the LOWESS algorithm [6] to obtain the broadband noise of the measured signal. The measured data points are analysed by assigning a weighting factor to each point in the plot, determined by a weighting function that is selected based on the characteristics of the data and possesses specific properties. A fitted value is then computed for each measured point using weighted least squares regression, corresponding to a polynomial fit. Subsequently, new weights are calculated based on the difference between the measured data points and fitted values. Small residuals are assigned larger weights, while large residuals receive smaller weights, thereby reducing the influence of outliers in the iterative fitting process. Finally, the sound pressure level spectra $re\, 2\text{x}10^{-5}$ Pa was calculated. The results shown in this work only refer to the microphone at the position at 90° for selected operating points.

4. Results

The results of the analysis of the acoustic measurements on a permanent magnet electric motor under load are presented in the form of sound pressure level spectra. Effects of different load conditions on the noise radiation of electric motors can be examined in the spectra achieved from the uncorrected signals.

Due to the general categorization of the measurements into two groups, the analysis is separated into two categories as well. In the following, the findings for the measurements at constant torque with varying speeds will be presented in Section 4.1 and in Section 4.2 for constant speed at varying torques.

4.1. Constant torque

The first scenario investigated the motor's sound radiation at two constant loads, $M = 0$ Nm and $M = 60$ Nm, each tested at four different speeds. Measurements for the first condition were taken in idle mode with the test motor disconnected from the load machine, thereby eliminating this particular external noise source. The sound pressure level spectra are presented in Figure 3a, for the far-field sound pressure level obtained by the microphone at 90°. The spectra show broadband noise, which decreases with increasing frequency. No significant differences in the broadband noise levels were observed across the different rotational speeds. Notably, a dominant tone at 174 Hz is present in the spectra in the background noise measurement recorded with the motor off, indicating that it originates from sources other than the motor itself. Therefore, this frequency component is not attributable to motor induced acoustic radiation. The background noise exhibits a higher broadband level than any of the individual speed measurements in the low frequency region up to about 1 kHz.

As expected, the dominant tones shift to higher frequencies for increasing rotational speeds because the fundamental rotational frequency increases as well. The spectra all exhibit prominent peaks at the 48th multiple of the corresponding fundamental mechanical frequency. This can be attributed to various mechanisms, as illustrated in Table 4.1, such as the 2nd or 6th harmonic of the rotor space harmonics or a multiple harmonic caused by cogging torque or torque ripples, for which the fundamental frequency is $f_{rip} = 6 \cdot n \cdot f_{me}$ with n = 1,2,3 and f_{me} the mechanical frequency [7]. Notably, the level of the peak increases with increasing rotational speed, except for $n_4 = 7800\,\text{min}^{-1}$, where the level decreases compared to $n_3 = 6000\,\text{min}^{-1}$. The highest amplitudes in the spectra regarding motor noise are observed for n_3 and n_4, with levels of approximately 60 dB and 61 dB at frequencies of 585 Hz and 390 Hz, respectively. Notably, the frequency 585 Hz exhibits a special behaviour, as it is a prominent peak independent of the rotational speed, except for n_4. Excluding the measurement at 7800 min-1 it can be assumed that the frequency of 585 Hz is caused by a noise source other than the motor. However, the level of the tone increases with increasing speed, which indicates an indirect influence of the motor.

Figure 3b shows the spectra for the cases with a constant load of 60 Nm. The most significant difference compared to the results obtained at idle is the increasing broadband noise for increasing rotational speeds. This can be explained by the fact that the power P introduced by the torque M and the angular frequency ω is given by $P = M \cdot \omega$. As a result, the radiated

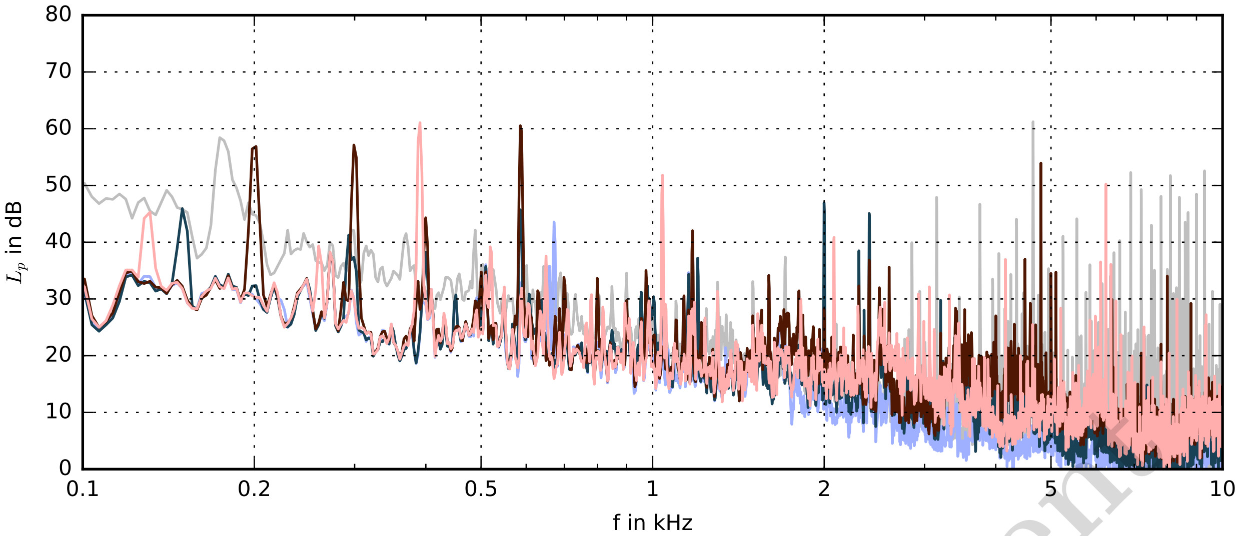

(a) Sound pressure level spectra for constant load $M = 0\,\mathrm{Nm}$ at different speeds.

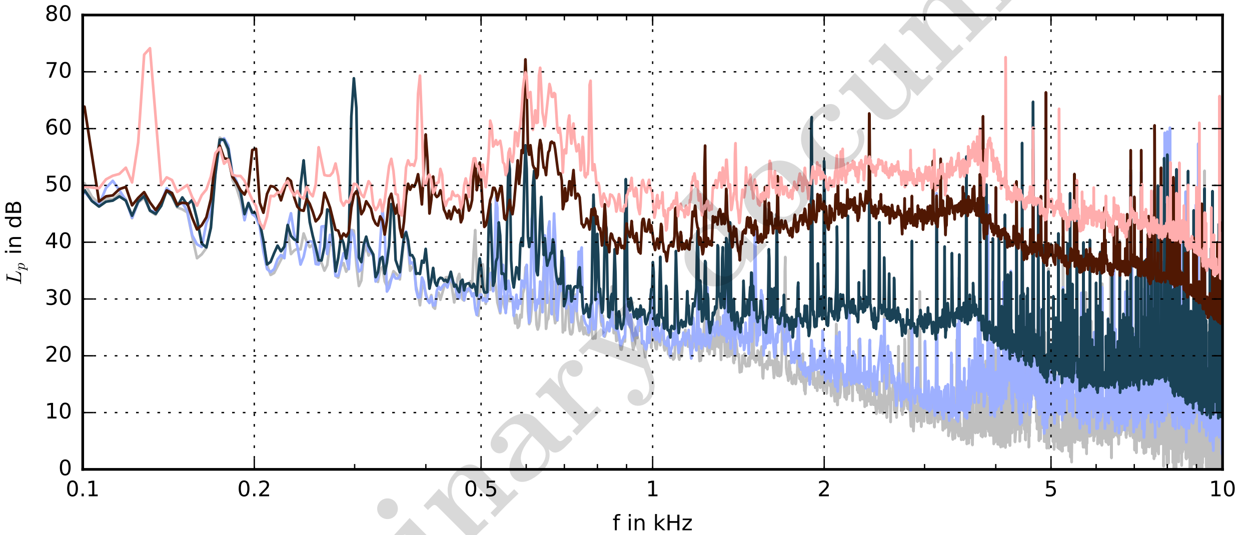

(b) Sound pressure level spectra for constant load $M = 60\,\mathrm{Nm}$ at different speeds.

Figure 3: Sound pressure level spectra for constant load at different rotational speeds for the measured signals without any use of the mentioned correction methods.($n_1 = 840\,\mathrm{min}^{-1}$; $n_2 = 3000\,\mathrm{min}^{-1}$; $n_3 = 6000\,\mathrm{min}^{-1}$; $n_4 = 7800\,\mathrm{min}^{-1}$).

sound power also increases, which is visible in the spectrum as an increase in the broadband component. It is also worth noting that the load machine was running during the measurement to achieve the required operating points during test and was measured by the microphones accordingly. Consequently, tones radiated by the load machine may also be included in the spectra.

However, the prominent peaks can be seen independently of the load condition. As described for the background noise measurement in Figure 3a, the most prominent tone at 174 Hz has nearly constant level of about 58 dB, independent of the speed. The most dominant peak occurs for $n_4 = 7800\,\mathrm{min}^{-1}$ at 130 Hz with 74 dB. It represents the fundamental mechanical frequency. The main source of torque ripple noise is the 6th harmonic of the fundamental mechanical frequency, which produces the highest amplitudes across all speeds, as shown in the spectra. Moreover, 8 k^{th} orders harmonics appear, such as 24^{th}, 32^{th}, 40^{th} since the motor has 8 poles. Especially for $n_2 = 3000\,\mathrm{min}^{-1}$ and $n_3 = 6000\,\mathrm{min}^{-1}$ the 38^{th} harmonic order frequencies, 1900 Hz and 3800 Hz, are prominent due to rotor dynamic eccentricity [9]. Interesting at this point is that the amplitude of the tones stays constant for the different rotational speeds at 62 dB. The assumption that rotor dynamic eccentricity has no speed dependence on sound pressure level cannot be confirmed

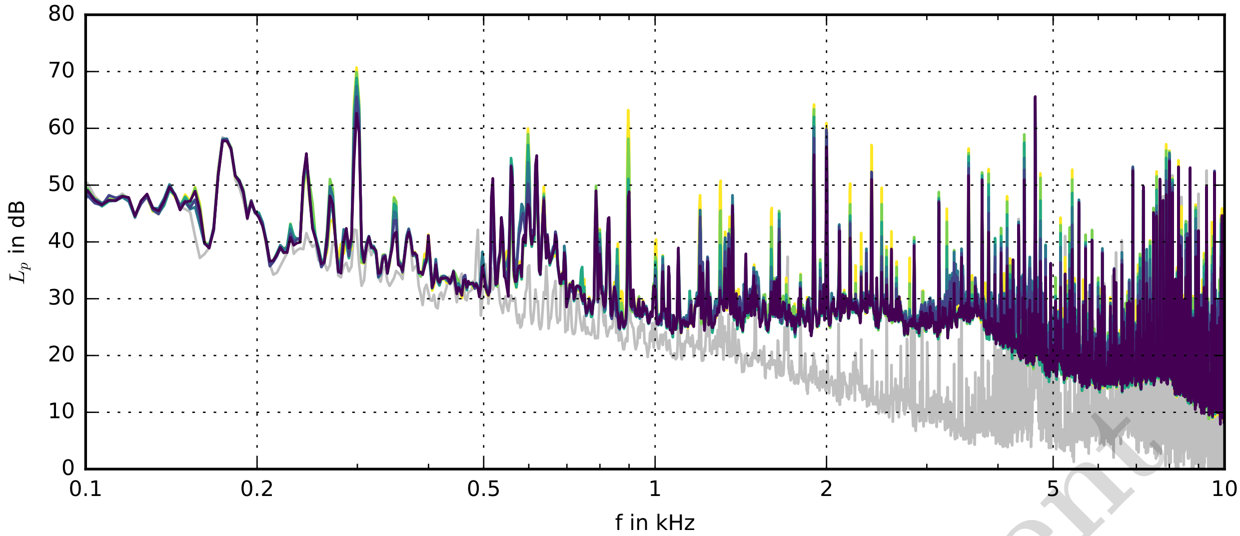

Figure 4: Sound pressure level spectra for constant speed $n_2 = 3000\,\text{min}^{-1}$ at different torques. (— $M = 15\,\text{Nm}$; — $M = 30\,\text{Nm}$; — $M = 45\,\text{Nm}$; — $M = 60\,\text{Nm}$; — $M = 75\,\text{Nm}$; — $M = 90\,\text{Nm}$;)

for the 2nd-order harmonic at 7600 Hz for n_3 and 9880 Hz for n_4. In this case the sound pressure level increases by 5 dB for the higher speed. In addition, the effect of bearing passing could be assumed for high speeds, especially for $n_4 = 7800\,\text{min}^{-1}$ at 634 Hz, which represents the fractional order 4.8 of the mechanical frequency [9].

Figure 5 shows the overall sound pressure level for constant loads $M = 60\,\text{Nm}$ and $M = 90\,\text{Nm}$ for different speeds. It is shown that the overall sound pressure level increases for increasing speed. The graph shows a non linear relation regarding the rotational speed and the sound pressure level, as doubling the speed from $n_2 = 3000\,\text{min}^{-1}$ to $6000\,\text{min}^{-1}$ leads to an increase in the level by about 5 dB, whereas from $6000\,\text{min}^{-1}$ to $7800\,\text{min}^{-1}$ there is an increase by about 7 dB for $M = 60\,\text{Nm}$ and about 10 dB for $M = 90\,\text{Nm}$. This is likely caused by the relationship between the excitation forces in the air gap and the structural natural frequencies. When the frequencies of the excitation forces are close to the structural natural frequencies, resonance phenomena occur at the corresponding mode. These natural frequencies are associated with specific structural modes, which radiate sound into the surrounding environment with varying power. The relationship between the sound power levels of the modes and the amplitudes of the excitation forces is not linear. In addition, background noise sources may also affect the overall sound pressure level obtained here.

4.2. Constant speed

The second scenario investigates how different load conditions affect the noise radiation by keeping the speed constant. Therefore, two different speeds are chosen and tested for six different torques each, according to Table 3. The results are shown in Figure 4.

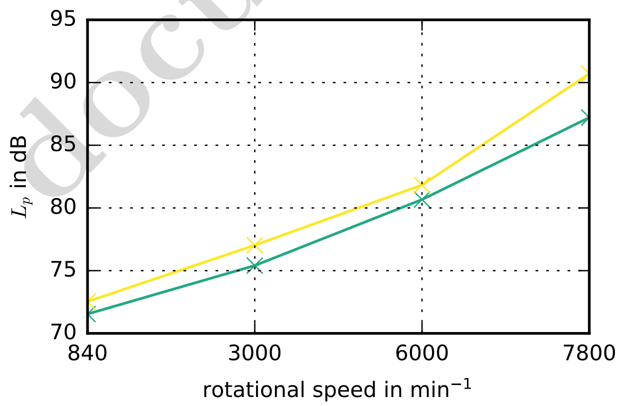

Figure 5: Overall sound pressure level for constant torque — $M = 60\,\text{Nm}$ and — $M = 90\,\text{Nm}$ at different speeds obtained from the sound pressure level spectra for 100 Hz $\leq f \leq$ 10 kHz.

The most prominent difference to the constant torque scenario is that the broadband noise seems to be unaffected by increasing torque but increases compared to the configuration with no load (idle). The dominant tones of the spectra shown in Figure 4 are similar to those in the corresponding graphs of the same speed in Figure 3a and Figure 3b, which enables a more detailed look at the effect of different loadings on the sound pressure level of certain tones. A general trend can be observed whereby the amplitudes of the tones increases, as the torque increases for example at 1900 Hz. The sound pressure levels increase compared to the lowest torque at M=15 Nm by 3 dB, 5 dB, 7 dB, 8 dB and 9 dB in accordance with the corresponding torques. Figure 6 shows the overall sound pressure level for constant speed at increasing load. The graph

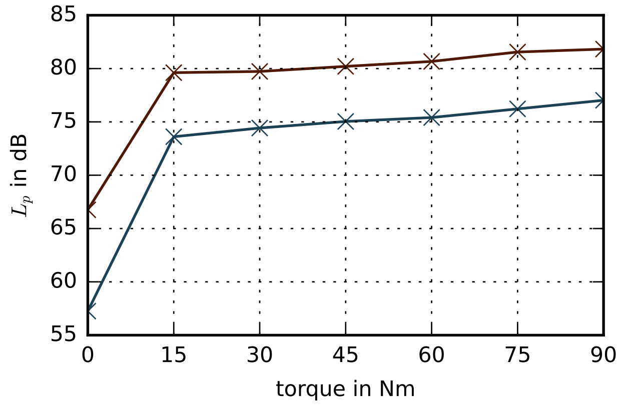

Figure 6: Overall sound pressure level for constant speed (— $n = 3000\,\text{min}^{-1}$; — $n = 6000\,\text{min}^{-1}$) at different loads obtained from the sound pressure level spectra for $100\,\text{Hz} \leq f \leq 10\,\text{kHz}$.

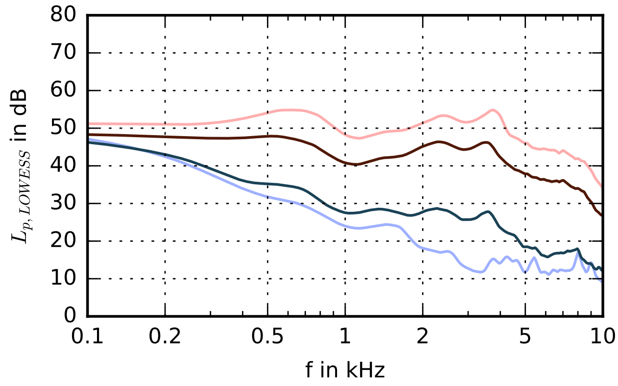

Figure 7: Sound pressure level spectra for constant load $M = 60\,\text{Nm}$ with varying speed for the broadband noise obtained with the LOWESS algorithm. (— $n = 840\,\text{min}^{-1}$; — $n = 3000\,\text{min}^{-1}$; — $n = 6000\,\text{min}^{-1}$; — $n = 7800\,\text{min}^{-1}$)

indicates increasing levels for increasing loads for both speeds. Although, as mentioned before, there is a general higher amplitude for higher speeds. The increase in the sound pressure level seems to be similar for both speeds. It can be observed that for an increase by 15 Nm the level increases by 1 dB.

Finally, in Figure 7 the results for the broadband noise at constant load $M = 60\,\text{Nm}$ for different speed obtained with the LOWESS algorithm is shown. As discussed in previous sections, the method uses a locally weighted regression and smoothing operation to remove local peaks in the spectra. The results show a good approximation for the broadband noise of the measured signal. The general trend of higher rotational speeds leading to an increase in broadband noise, which was derived from Figure 3b, can be verified. It can be seen that the measured speeds can be separated into two groups for which the difference in the level increases to higher frequencies.

5. Conclusion

This study experimentally investigates the noise contribution of an electric drive train in urban air mobility vehicles, using a representative electric motor. Significant noise mechanisms of the electric motor have been observed under various operating conditions, despite the challenging acoustic environment during the measurements. The results indicate that, as the load increases, the radiated noise of the motor increases in a non-linear relation. Increasing torque leads to an increase in the level of tonal components while the broadband noise remains unchanged. Increasing speed amplifies both tonal and broadband noise. The most dominant noise mechanisms are linked to torque ripple, dynamic rotor eccentricity and rotor and stator harmonics indicated as integer multiples of the fundamental mechanical frequency. Additionally, fractional orders were found at high rotational speeds which could be interpreted as the bearing passing frequency of the rotor.

References

[1] S. Schade et al., "Conceptual design of electrically powered urban air mobility vehicles for psychoacoustic studies," *Aerospace*, vol. 13, no. 4, 2026.

[2] S. Hakansson et al., "Numerical investigation of the noise generation of electric motors in urban air mobility vehicles," *Journal of the Acoustical Society of America*, vol. 159, 2025.

[3] S. E. H. GmbH, *Datasheet sy43.b rev5*, `https://sci-mo.de/`. Accessed: 2026-29-05, 2024.

[4] P. Welch, "The use of fast fourier transform for the estimation of power spectra: A method based on time averaging over short, modified periodograms," *IEEE Transactions on audio and electroacoustics*, vol. 15, no. 2, pp. 70–73, 1967.

[5] J. S. Bendat et al., *Random Data: Analysis and Measurement Procedures*. Hoboken: John Wiley & Sons, 2010.

[6] W. S. Cleveland, "Robust locally weighted regression and smoothing scatterplots," *Journal of the American statistical association*, vol. 74, no. 368, pp. 829–836, 1979.

[7] T. Sun et al., "Effect of pole and slot combination on noise and vibration in permanent magnet synchronous motor," *IEEE Transactions on Magnetics*, vol. 47, no. 5, pp. 1038–1041, 2011.

[8] K. Fröhlingsdorf, "Automatisierte Trennung und Zuordnung von Geräuschanteilen im Innenraum von Elektrofahrzeugen," Ph.D. dissertation, RWTH Aachen, 2023.

[9] F. Lin et al., "Noise prediction and sound quality analysis of variable-speed permanent magnet synchronous motor," *IEEE Transactions on Energy Conversion*, vol. 32, no. 2, pp. 698–706, 2017.